Theoretical AIM and ELI-D Study of Ammonium Hexahydrohexaborate

ARTICLE *in* ZEITSCHRIFT FÜR ANORGANISCHE UND ALLGEMEINE CHEMIE · SEPTEMBER 2013

Impact Factor: 1.16 · DOI: 10.1002/zaac.201200489

4 AUTHORS, INCLUDING:

Stefan Mebs
Freie Universität Berlin
54 PUBLICATIONS **516** CITATIONS
SEE PROFILE

Julian Henn
University of Bayreuth
55 PUBLICATIONS **1,078** CITATIONS
SEE PROFILE

Dieter Lentz
Freie Universität Berlin
315 PUBLICATIONS **3,867** CITATIONS
SEE PROFILE

DOI: 10.1002/zaac.201200489

Theoretical AIM and ELI-D Study of Ammonium Hexahydrohexaborate

Stefan Mebs,*[a] Julian Henn,[b] Peter Luger,[a] and Dieter Lentz*[a]

Keywords: Electron density; Boranes; Atoms In Molecules; Electron Localizability Indicator; Charge transfer

Abstract. The theoretically obtained electronic properties of ammonium hexahydrohexaborate are analyzed by means of Atoms In Molecules (AIM) Theory and Electron Localizability Indicator (ELI-D). For AIM, the electron density (ED) derived from a calculation under periodic boundary conditions and subsequent modeling of the theoretical structure factors is compared to direct analysis of the ED from gas-phase calculations of packing schemes. Both procedures lead to similar physical properties. The quality of the theoretical multipole model is additionally confirmed by a detailed qualitative and quantitative analysis of the residual densities. $(B_6H_6)^{2-}$ is not stable in the gas phase. Considering the ELI, this leads to a large distance of the B–B valence basin attractor to the B–B axis. This outwardly curved localization is a sign for a weak B–B interaction. The structure is stabilized in the crystal by an unusual intermolecular contact between the protic hydrogen atoms of ammonium and the centers of the B–B–B triangles of the $(B_6H_6)^{2-}$ octahedron. All common real space bond descriptors, such as the Laplacian, the energy densities, the delocalization index, and the source function (including local source) classify this bond type as being of closed-shell character.

Introduction

The bonding patterns in deltahedral borane cages cannot be explained by the Lewis electron pair model.[1] Starting with the fundamental works of *Lipscomb*[2] and *Wade*,[3] large progress was made in the last 50 years in understanding these compounds theoretically.[4–9] For the understanding of chemical bonding, detailed information about the physical properties of any given system is needed. An essential source of information is the distribution of the electron density (ED) between the nuclei.[10] The ED may be obtained either by high-level theoretical calculations with periodic boundary conditions or by high-resolution X-ray diffraction at low to very low temperatures and subsequent modeling of the ED using a multipole formalism, such as provided by *Stewart* in 1969[11] and extended by *Hansen* and *Coppens* in 1978.[12] In the last decades, experimental electron density determinations of several deltahedral boranes have been performed.[13–26] A detailed theoretical AIM-study on several daltahedral boranes was provided in the early 1990's by *Bader* and *Legare*.[27]

In this work, starting from the experimental structure of a high-resolution X-ray data set,[28] (Figure 1A) theoretical calculations were performed for the smallest *closo*-borate, $(B_6H_6)^{2-}$, both for periodic boundary conditions (model *cry*) and for gas phase clusters including the first and second coordination sphere (models *pck*-s and *pck*-l, respectively) around the formal $(B_6H_6)^{2-}$ anion, see Figure 1B and C. Detailed information of the model generation is provided in the last section.

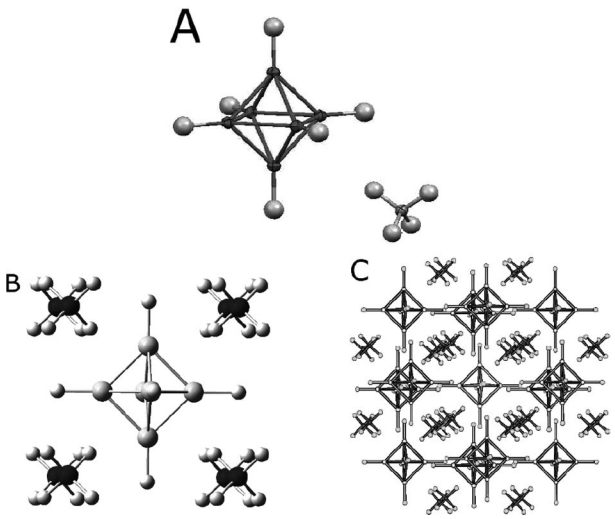

Figure 1. (A) Experimental structure of $(B_6H_6)^{2-}\cdot 2NH_4^+$; (B) First coordination sphere of $(B_6H_6)^{2-}$ (*pck*-s); (C) Large packing scheme (*pck*-l). The central molecules (light grey) were analyzed.

The electron density distribution is analyzed by means of Atoms In Molecules theory (AIM)[29,30] and stockholder partitioning (Hirshfeld surfaces, HS).[31,32] The conventional interpretation of the AIM bond topology is thereby supported by analysis of integrated bonding descriptors such as the delocalization index (δ(x,y)),[33,34] the integrated amount of electrons

* Dr. S. Mebs
E-Mail: stebs@zedat.fu-berlin.de
* Prof. Dr. D. Lentz
Fax: +49-30-838-53310
E-Mail: dlentz@zedat.fu-berlin.de
[a] Institut für Chemie und Biochemie/Anorganische Chemie
Freie Universität Berlin
Fabeckstr. 34–36 and 36a
14195 Berlin, Germany
[b] Laboratory of Crystallography
Universität Bayreuth
95440 Bayreuth, Germany

Supporting information for this article is available on the WWW under **http://dx.doi.org/10.1002/zaac.201200489** or from the author.

within the zero flux surface (N_{zfs}), and the source function (SF)[35,36] (including local source (LS)[37]). Moreover, the investigation of the Electron Localizability Indicator (ELI-D)[38] is included, as these integrated real-space indicators show a typical behavior for multicenter bonds, which allows the discrimination from conventional 2e2c-bonds.[26] As δ(x,y), N_{zfs}, and ELI-D cannot (yet) be derived from experimental data this analysis essentially complements experimental results. The SF quantifies the atomic contributions to the ED of any reference point; this also includes atoms, which are not directly connected to the reference point. In such way, delocalization effects can be described with absolute numbers. This is also possible with δ(x,y), introduced by *Bader* and *Stephens*. The ELI-D is a further development of the electron localization function[39,40] (ELF). ELF and ELI divide the space into regions of localized electron pairs instead of atoms and therefore greatly complement the AIM theory. The partitioning is done in analogy to the topological analysis performed in AIM. Thus, the partitioning is space filling and discrete, providing reliable integrated electron numbers of both, core shells and (non)bonded valence electrons.[41] Valence basins connecting two core basins are called disynaptic, whereas lone pairs and hydrogen atoms exhibit so-called (protonated) monosynaptic valence basins. The disadvantageous reference of the ELF formalism to the uniform electron gas was overcome with the introduction of the ELI-D. The ELF was widely applied to borane compounds in order to understand delocalization effects,[42–45] but quantitative analyses are rare.[46]

A topological analysis of deltahedral boranes[27] applying AIM reveals that the valence density is generally delocalized over the B–B–B (and B–H–B) ring surfaces. This leads to small values of the ED ($\rho(\mathbf{r})$) between two adjacent nuclei (e.g. at the bond critical points, bcp) of about $\rho(\mathbf{r}_{bcp}) = 0.8$ e·Å^{-3} accompanied by comparably large values of about $\rho(\mathbf{r}_{rcp}) = 0.7$ e·Å^{-3} in the ring centers (e.g. at the ring critical points, rcp). Moreover, the flat shape of the valence density leads to small negative values of the Laplacian at the bcp [$\nabla^2\rho(\mathbf{r}_{bcp})$] and substantially large B–B bond ellipticities (ε). The most prominent feature of localization functions with respect to deltahedral borane chemistry is that regions of high localization have the form of the dual polyhedron of the boron cages.[42] $(B_6H_6)^{2-}$ is an octahedron, thus a cube with its corners lying above the centers of the B–B–B planes is the corresponding dual polyhedron. Recently, two combined experimental and theoretical studies were published including the larger homologues $(B_{10}H_{10})^{2-}$ and $(B_{12}H_{12})^{2-}$ and two *arachno*-boranes.[26,27] Despite the complex bonding patterns, especially in the lower-symmetrical *arachno*-boranes, the authors found a linear relation of $\rho(\mathbf{r}_{bcp})$ against the B–B distances. Moreover, a linear relation of the electron populations within the ELI-D basins against the basin volumes was found. Both relations are confirmed by the actual study and may serve as a benchmark for later studies.

The title compound exhibits an intermolecular contact with an unusual bond path – the protic hydrogen atoms of $(NH_4)^+$ point towards the B–B–B ring plane of $(B_6H_6)^{2-}$ – which was quantified and characterized. Finally, the charge separation between the $(B_6H_6)^{2-}$ dianion and the $(NH_4)^+$ cations was determined.

Results and Discussion

ED-derived Properties

Table 1 and Table 2 display all relevant topological features of the ED. The atomic charges of the B, H(B), N, and H(N) atoms, which correspond to the atomic volumes confined to the 0.001 a.u. density isosurfaces (Q_{001}) are given in Table 3.

Table 1. Topological bond descriptors[a] (Part 1).

Bond	Model	$\rho(\mathbf{r}_{bcp})$ /e·Å^{-3}	$\nabla^2\rho(\mathbf{r}_{bcp})$ /e·Å^{-5}	d /Å
B–B	*cry*	0.83	–2.0	1.730
	pck-l	0.84	–2.9	1.734
	pck-s	0.84	–2.9	1.734
B–H	*cry*	1.13	–4.5	1.196
	pck-l	1.16	–5.3	1.196
	pck-s	1.17	–5.3	1.196
N–H	*cry*	2.22	–34.0	1.035
	pck-l	2.20	–41.9	1.035
	pck-s	2.21	–42.5	1.035
rcp	*cry*	0.77	–0.3	–
	pck-l	0.77	–0.2	–
	pck-s	0.76	–0.2	–
ccp	*cry*	0.43	6.3	2.447
	pck-l	0.45	6.3	2.452
	pck-s	0.45	6.2	2.452
cage···H(N)	*cry*	0.11	1.5	2.527
	pck-l	0.12	1.0	2.520
	pck-s	0.12	1.0	2.520

a) For all bonds, $\rho(\mathbf{r}_{bcp})$ is the ED at the bcp; $\nabla^2\rho(\mathbf{r}_{bcp})$ is the corresponding Laplacian; d is the interactomic distance (bcp) and the intracage B–B distance (ccp), respectively.

Table 2. Topological bond descriptors[a] (Part 2).

Bond	Model	d_1 /Å	λ_3 /e·Å^{-5}	ε
B–B	*cry*	0.865	2.19	2.56
	pck-l	0.867	1.60	2.04
	pck-s	0.867	1.66	2.05
B–H	*cry*	0.532	10.33	0.00
	pck-l	0.527	11.55	0.00
	pck-s	0.526	11.35	0.00
N–H	*cry*	0.745	24.82	0.01
	pck-l	0.774	18.80	0.00
	pck-s	0.776	18.69	0.00
rcp	*cry*	1.006	1.32	–
	pck-l	1.006	1.45	–
	pck-s	1.006	1.42	–
ccp	*cry*	1.223	2.09	–
	pck-l	1.226	2.09	–
	pck-s	1.226	2.05	–
cage···H(N)	*cry*	1.721	1.61	0.01
	pck-l	1.708	1.54	0.00
	pck-s	1.709	1.54	0.00

a) For all bonds, d_1 is the distance from the first atom to the bcp; for rcp and ccp d_1 is the average distance to the ring or cage constitutive B atoms; λ_3 is the curvature of the ED along the interatomic axis; ε is the bond ellipticity [$\varepsilon = (\lambda_1/\lambda_2)-1$; $\lambda_1 > \lambda_2$].

Due to symmetry restrictions, the 12 B–B bcps are identical. The same is true for all other types of critical points. Table 1

Zeitschrift für anorganische und allgemeine Chemie ZAAC Journal of Inorganic and General Chemistry

Table 3. Atomic AIM charges.

Model	Q_{001} B /e	Q_{001} H(B) /e	Q_{001} H(N) /e	Q_{001} N /e
cry	0.39	–0.65	0.40	–0.78
pck-l	0.33	–0.61	0.44[a)]	–1.01
pck-s	0.36	–0.59	0.44[a)]	–0.92

a) Hydrogen atom, which points towards the central B_6H_6 cage.

and Table 2 also include the weak intermolecular interaction between the protic hydrogen atoms and the borate. Apparently, the overall agreement of the topology is very good between all models. The B–B bond of all models perfectly match the relation of $\rho(\mathbf{r}_{bcp})$ vs. B–B bond lengths, which was found for other borane cages[26] and the rcp-topology perfectly matches the relation of $\rho(\mathbf{r}_{rcp})$ vs. d_1. The charge of the $(B_6H_6)^{2-}$ anion is –1.6 to –1.7 e. The value of about –1.4 e for model *pck*-s has to be considered with care, since the calculated cluster is small, highly charged and each ammonium is connected to only one borate.

Figure 2A and B shows the static deformation density (sdd) and Laplacian isosurface representations for the $(B_6H_6)^{2-}$-part in the model *cry*. The sdd exhibits the expected cube-like shape. For the Laplacian, weak valence shell charge concentrations (vscc) are found between adjacent boron atoms in borane cages as expected[26] (see Figure 6B for exact locations (model *pck*-s)). In Figure 2C and D, the electrostatic potential (ESP) and the ED are mapped onto the Hirshfeld surface (HS) of the borate. One finds an accumulation of ED in the center of the B–B–B triangles instead of three equivalent accumulations along the N–H···B axes as one might have expected. This result is supported by the intermolecular bond topology, see below. In Figure 2E–H, the corresponding surfaces are given for the ammonium ion.

The considerably high overall-agreement between the theoretically obtained multipole model *cry* and the multipole-free models *pck*-s and *pck*-l supports the assumption of a sufficient reliability of the derived physical properties and the underlying ED.

Residual Density Analysis

A comparative residual density analysis of all subsequent refinement steps helps to identify a suitable multipole model and to prevent over modeling. The refinement of multipole parameters against structure factors from periodic boundary conditions calculations has two principal limitations: The restricted choice of methods and basis-sets for the calculation of the periodical wavefunctions and the ambiguities[47] and limitations[48–50] of the multipole-model itself. In order to quantify these limitations, an analysis of several refinement steps was done for model *cry*, for which experimental errors are irrelevant. Additionally, a further refinement step including all multipole and expansion parameters simultaneously is given (*cry*-all). Since this model is not convergent, the ED-derived properties were obtained from model *cry*-final. Table 4 lists the conventional suitability index R_1 together with several residual density descriptors: the flatness of the residual density ($\Delta\rho_0 = \rho_{0,max} - \rho_{0,min}$), the fractal dimension of the residual density value zero ($d^f(0)$), which expectation value for a

Table 4. Measures for refinement quality and residual density distribution in model *cry*.

Step[a)]	R_1	$\Delta\rho_0$ /e•Å^{-3}	$d^f(0)$/POF /%	e_{gross} /e
scale	2.47	1.3574	2.4568/2.7	14.505
multi	0.77	0.2028	2.5029/0.8	3.787
final[b)]	0.64	0.1467	2.5140/0.4	2.892
all	0.49	0.1548	2.5027/0.8	1.989

a) "scale": only scale factor refined; "multi": refinement of multipoles; "final": blockwise refinement of κ and κ_0; "all": multipoles and expansion parameters are refined altogether. b) The ED-derived properties (see previous section and next section) were obtained from this model.

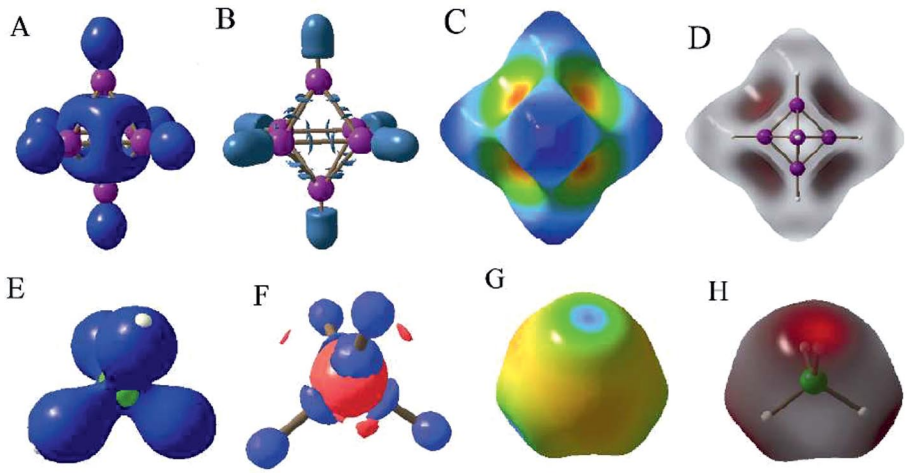

Figure 2. (A) Static deformation density of $(B_6H_6)^{2-}$ at an isosurface value of 0.15 e•Å^{-3}; (B) Laplacian of the ED at an isocontour value of –3.75 e•Å^{-5}; (C) Electrostatic potential mapped on the Hirshfeld surface, values range from –0.70 (blue) to –0.35 (red) e•Å^{-1}; (D) ED mapped on the Hirshfeld surface, values range from 0.0 to 0.3 e•Å^{-3}; (E–H) Corresponding results for $(NH_4)^+$; (F) Isosurface values of –35 (blue) and 10 (red) e•Å^{-5}; (G) Values range from 0.29 (yellow) to 1.60 (blue) e•Å^{-1}.

Special Issue

Gaussian distribution of residuals can be calculated analytically as a function of the experimental resolution and the chosen residual density grid,[51] the Percentages of Features (POF), which is calculated from observed and expected $d^f(0)$, where again the expected value is calculated from the reciprocal resolution and the residual density grid dimensions; a small part of the POF is due to statistical fluctuations, however, typical values of the POF for random residual density grids are about 0.03 %.[51] Finally, the gross residual electrons (e_{gross}), which give a total absolute error of the model inadequacies and noise are listed. As one can see, the results never exactly match the values for ideal data with an ideal model.

Figure 3 displays residual density statistics, such as the probability distribution histogram (pdh), the normal probability plot (npp),[52] and the fractal dimension plot (fdp)[53] for the refinement steps in model *cry*.

Figure 3A–C displays the residual density distribution (rdd) in terms of pdh, npp, and fdp for the initial scale factor refinement of model *cry*. Since the model is spherical at this point, extended positive and negative residuals are expected and found. Refinement of multipoles with the restriction of the initial charge separation between borate and ammonium leads to the results presented in Figure 3D–F. Although the absolute numbers are much smaller for all plot-types (see legend), the residuals obviously still include systematic effects, which are not described yet. The statistics given in Figure 3G–I result after release of the initial charge separation, inclusion of κ for the boron and nitrogen atom, and blockwise refinement of κ and κ_0 for all atoms (B, H(B), N, H(N)). The residuals are much less systematically distributed than before, but still not featureless. The combined refinement of multipole and expansion parameters (*cry*-all) leads to the lowest crystallographic agreement factor and smallest number of gross residual electrons, however, from the twice as large POF value of 0.8 % compared to 0.4 % in model *cry*-final it is seen that the better agreement is achieved at the expense of more features in the residual density distribution. Moreover, $\Delta\rho_0$ is slightly higher in model *cry*-all. Therefore, this is not a suitable model. If, for example, the theoretical structure factors are somewhat biased by the choice of basis-sets, it might be better to have this "information" in the residuals than in the model, from which the ED-derived properties finally will be obtained. Inspection of the rdd after final refinements of theoretical data (*cry*) visualizes the limitations of the multipole description (see Figure 4).

In fact, the absolute values are very small (isocontours at $\pm$0.025 e•Å^{-3}), but the residuals are still not featureless. Small holes are seen on all atoms, small peaks are seen along all N–H and B–H bonds as well as in the B–B–B triangles. As long as these effects are smaller than the chemical effects, the problem might be negligible. This argument, however, becomes questionable for the interpretation of weak intermolecular interactions with a $\rho(r_{bcp})$ value of about 0.1 e•Å^{-3}.

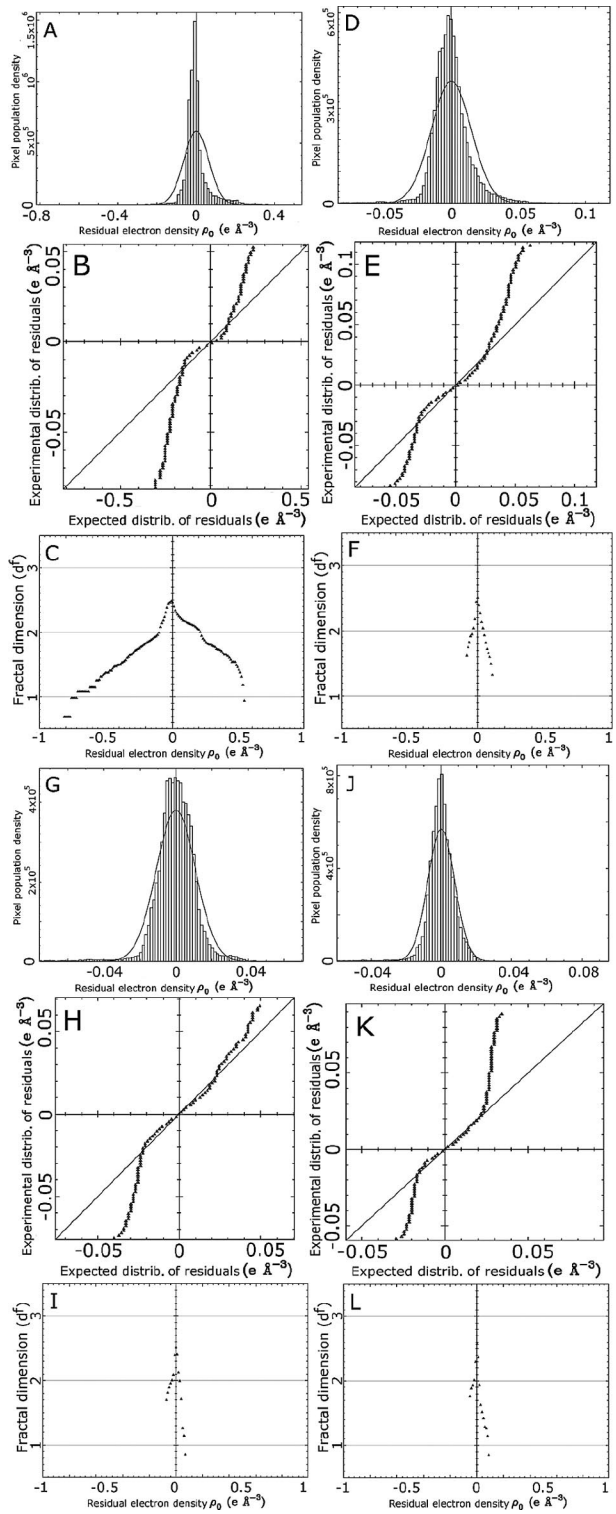

Figure 3. Probability distribution histogram (pdh), normal probability plot (npp), and fractal dimension plot (fdp) of model *cry*. (A–C) Initial scale factor refinement; (^{d}–F) Refinement of multipoles; (G–I) Release of charge separation between anion and cation, inclusion of κ for N and B atoms; subsequent blockwise refinement of κ and κ_0 for all atoms [B, H(B), N, H(N)]; (J–L) Combined refinement of multipoles and expansion parameters. Residual densities (x axes) range from –0.80 e•Å^{-3} to 0.50 e•Å^{-3} (first row); –0.08 e•Å^{-3} to 0.12 e•Å^{-3} (*cry*-multi, second row); –0.08 e•Å^{-3} to 0.08 e•Å^{-3} (*cry*-final, third row); –0.08 e•Å^{-3} to 0.09 e•Å^{-3} (*cry*-all, fourth row).

Intermolecular Interactions and the ELI-D

The electron populations [N_{001}(ELI)] and corresponding volumes (V_{001}(ELI)) of the disynaptic B–B valence basins,

Zeitschrift für anorganische und allgemeine Chemie ZAAC Journal of Inorganic and General Chemistry

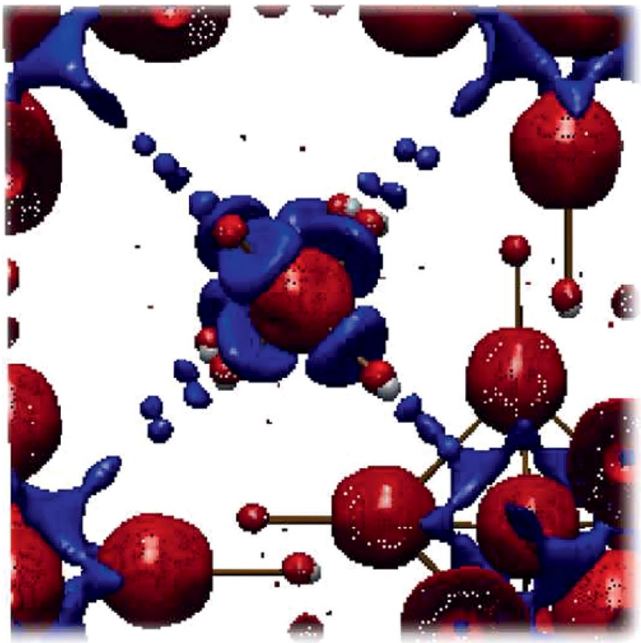

Figure 4. Isosurface representation of the residual density distribution of model *cry* at ±0.025 e•Å^{-3}.

V_2(B,B), are 1.04 e and 3.13 Å^3 (model *pck*-s). These values perfectly match the linear relation, which was found for N_{001}(ELI) against V_{001}(ELI) in a former study including gas-phase calculations of borane and borate cages.[26] The presence of the ammonium ions obviously does not influence this population significantly, which indicates a rather weak intermolecular interaction. All B–B bonding descriptors of $(B_6H_6)^{2-}$, the ELI-D value at the V_2(B,B) attractor position (Y_D^a = 1.52, model *pck*-s), the delocalization index (δ(B,B) = 0.58, model *pck*-s), and the summed up integrated source contributions of the two direct bond partners (SF(B+B) = 0.44 e•Å^{-3} (53 %), model *cry*) are very close to the results of the B–B bond between central and apical B atoms of the bicapped square *anti*-prism in $(B_{10}H_{10})^{2-}$.[26] This leads to the assumption that the electronic properties of these B–B interactions are dominated by the (apical) boron atoms, which are located at the vertices of degree four. The distance of the attractor position to the B–B axis (Δ_{ELI}), however, is much larger (0.262 Å, model *pck*-s) than the typical values of disynaptic B–B valence basins as given in Ref. [26] (0.080 to 0.170 Å), which might be related to the fact that $(B_6H_6)^{2-}$ is not stable in the gas phase. The only example of a larger Δ_{ELI} value (0.329 Å) was found for a very small V_2(B,B) basin of $(B_{10}H_{10})^{2-}$[26] – it is the only one of the three V_2(B,B) types in this compound, for which no bcp is exhibited in the ED between the atoms. Δ_{ELI} may thus be related to the stability of the B–B interaction in cage structures. The sums of the electron populations of all core and (protonated) valence basins for the borate cage (model *pck*-s) yields a charge of –1.52 e (data cut at 0.001 a.u.), indicating a charge transfer from the dianion to the cations of about 0.48 e. For the AIM-charges, however, a slightly larger value (about 0.6 e) was found (see above). The difference originates in the different partitioning of space between AIM and ELI-D (although the *mathematical method* of partitioning is identical): The hydridic protonated valence basins, V_1(B,H), as well as the disynaptic B–B valence basins, V_2(B,B), of the borate slightly penetrate the protic AIM-H atoms, leading to a larger total charge for the borate in terms of ELI-D. Figure 5 displays the ELI-D at four different isovalues (model *pck*-s). The localization domain representations are double-coded with respect to the basin volumes in order to highlight the influence of intermolecular interactions on the sizes of the basins: The domains of small basins (basically core basins) are colored blue and are not transparent, whereas larger basins (basically protonated basins) are green and their transparency increases with size.

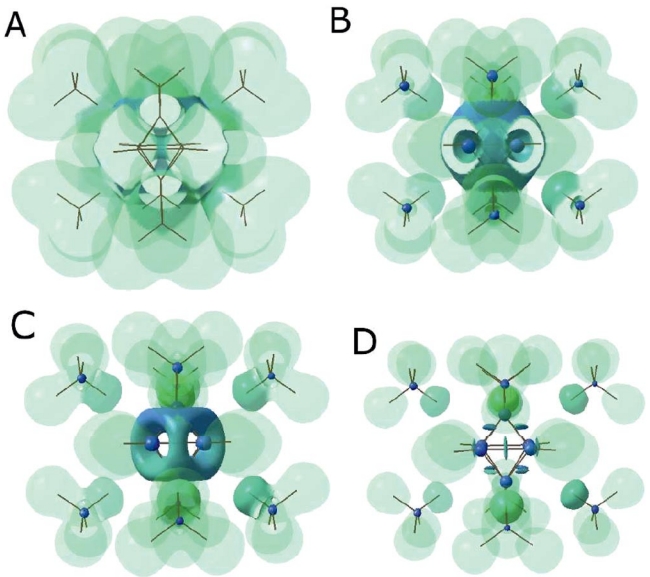

Figure 5. ELI-D representation of model *pck*-s at different isovalues. (A) Y_D^a = 0.60; (B) Y_D^a = 1.00; (C) Y_D^a = 1.25; (D) Y_D^a = 1.50.

In Figure 5A (Y_D^a = 0.60) the basin connectivity between interacting protic valence basins and the B–B–B basins is visible. However, the localization domains of the protic and hydridic valence basins are already separated at this isovalue, which leads to the assumption that Hδ$^+$···Hδ$^-$ interactions (dihydrogen contacts) may be of minor importance in this structure, which is supported by the topology of the ED (see below). The interacting protic basins are significantly less transparent than those which are not involved in the cage···H(N) contact. In Figure 5B (Y_D^a = 1.00), the domains of dianion and cations are already separated. The dual polyhedron, which is known from deltahedral borane chemistry[42] becomes visible at Y_D^a = 1.25 (Figure 5C). The localization domains are still confluent at this isovalue and show a deep blue color (and no transparency), because they are also quite small (for more details, see Supporting Information). In Figure 5D (Y_D^a = 1.50), also the B–B valence domains split and show the attractor positions of the basins. They are located close to the B–B axes outside the molecular graph, which is consistent with earlier findings.[26]

The ED-topology of the cage···H(N) contact is quite unusual, as the H(N) atom seems to be topologically connected to the borate via the B–B–B rcp instead of being connected to

the hydridic hydrogen atoms (see Figure 6). Most probably the (N)H–B bond path comes extremely close to the B–B–B rcp without touching it. In this respect, the topology is qualitatively different to those of (T)M-cp(*) complexes, (T)M being a (transition)metal, cp(*) being the (decamethyl)cyclopentadienyl anion, for which a bond path is exhibited between the metal atom and each of the five carbon atoms.[54] For the cage···H(N) contact studied herein, one finds only one of the three expected bond paths connecting the rcp with a boron atom, which is also known from the (T)M-cp(*) complexes[55,56] but might also be due to program restrictions.[57] The rcp is located slightly outside the cage.

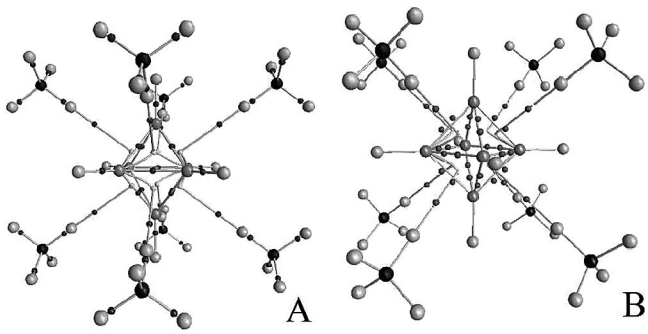

Figure 6. (A) Molecular graph of model *pck*-s including the intermolecular cage···H(N) contact and all types of critical points; small dark grey balls: bcp, small light grey balls: rcp. H(N) is seemingly topologically connected to the borate via the B–B–B rcp; (B) Locations of vsccs (for clarity all vsccs in the $(NH_4)^+$-regions are not shown). Quantitative values of $\rho(\mathbf{r}_{bcp})$ and $\nabla^2\rho(\mathbf{r}_{bcp})$ at the two cage···H(N) vs. ccs: 0.85 e·Å^{-3}, –4.1 e·Å^{-5} (close to rcp) and 0.15 e·Å^{-3}, 0.8 e·Å^{-5} (close to bcp).

The bcp from the theoretical calculation of this intermolecular contact has the following values for energy-density descriptors, which clearly classifies this type of interaction to be of closed-shell character:[58] $G/\rho(\mathbf{r}_{bcp})$: 0.54 a.u., $H/\rho(\mathbf{r}_{bcp})$: 0.02 a.u., –V/G: 0.96 a.u. (model *pck*-l). The interaction energy obtained by the relation $E = -1/2V$[59] is –12.03 kJ·mol^{-1}. As expected, the delocalization index between B and H(N) on the one hand and (B)H and H(N) on the other hand is very small: δ(B,H(N)) = 0.03 and δ(H(B),H(N)) = 0.01 (model *pck*-s). The values are significantly below those found for hydrogen bonds (about 0.10[60]) and still smaller than those found for weak dihydrogen contacts (0.04).[60] However, if one considers the B_3H_3 unit to interact with the protic hydrogen atom, a much larger value of δ(B_3H_3,H(N)) results. N_{zfs}[H(N),H(B)] is as large as 0.22 e (model *pck*-s), which is in the range of conventional hydrogen bonds.[60] Considering the integrated Source Function[35,36] (model *cry*), one finds the donor H(N) atom to have a contribution of –57.1 %, whereas the donor N atom supplies 52.6 % of the ED to the cage···H(N) bcp. Each of the three acceptor B atoms of the B–B–B-face has a contribution of –17.6 %; thus the three neighboring boron atoms together detract the ED at the cage···H(N) bcp by –52.8 %. The three corresponding hydridic H(B) atoms on the other hand have positive contributions of 14.6 % each (43.8 % altogether). These results are typical for weak isolated contacts.[36] However, since $\rho(\mathbf{r}_{bcp})$ at the cage···H(N) bcp is only 0.11–0.12 e·Å^{-3}, the results should be regarded with care.

Figure 7 displays the ED, the corresponding Laplacian (L) and the local source (LS) applied to several reference points (rp) along the crystallographic 111 direction, which includes the intermolecular cage···H(N) contact (model *cry*). The progressions start at the cage critical point (ccp) in the borate, passing the B–B–B-rcp, the cage···H(N)-bcp, and ending in the H(N) atom. We note that all functions are given on the same scale, since all discussed effects are very small. The LS is not only given for the rcp or the bcp as reference points, but furthermore for three points between the rcp and the bcp (at 1/4, 1/2, and 3/4 of the rcp-bcp distance). This procedure gives a more detailed impression of the electronic effects along this line compared to the restricted view to only one rp.

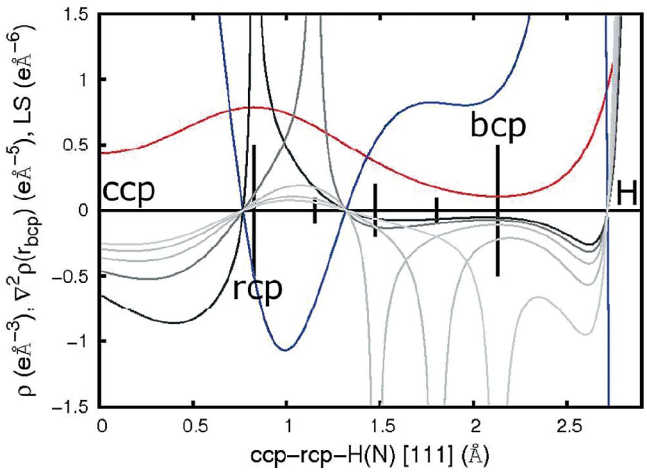

Figure 7. Line plot of the ED (red), the Laplacian of the ED (blue), and the local source (LS, grey) along the crystallograpic 111 direction, which includes the intermolecular cage···H(N) contact (model *cry*). Reference points (rp) are marked as black vertical lines. The dark grey LS-progression has the B–B–B rcp as rp, the light grey LS progression has the cage···H(N)-bcp as rp. Intermediate grey-levels refer to the three quarter points between rcp and bcp as rp.

The Figure is dominated by negative LS contributions along the line, only the region around the rcp and the region close to the H(N) atom supply ED to the chosen reference points. As expected, one finds a systematic decrease of electronic influence with increasing distance to the rp. The ED at the rcp is strongly influenced by the interior of the cage and little by the region around the cage···H(N)-bcp, see dark-grey line. On the other hand, the LS shows only small effects of the borate-cage to the cage···H(N)-bcp, see light-grey line. Besides this, a strong asymmetry is exhibited for the LS at the cage···H(N)-bcp, which stands for a high cage···H(N)-bcp bond polarity and confirms the closed-shell character of this weak interaction. This type of applying the LS to a set of reference points might be of general use for a more detailed description of different bond types in future studies.

Conclusions

The electronic situation of the $(B_6H_6)^{2-}$ anion very much resembles that of its higher analogue $(B_{12}H_{12})^{2-}$ in terms of

Zeitschrift für anorganische und allgemeine Chemie ZAAC Journal of Inorganic and General Chemistry

AIM topology and charges and in terms of the ELI-D, with the exception of the distance of the B–B ELI-D attractor position to the B–B axis (Δ_{ELI}). This parameter may thus be related to the stability of the B–B interaction in cage structures. In the crystal packing with ammonium $(B_6H_6)^{2-}$ shows an interesting and unique intermolecular contact between the protic hydrogen atoms of the ammonium and the B–B–B triangles, in which the B–B–B ring critical point is seemingly part of the intermolecular contact.

Disregarding the high symmetry within the crystal structure, the high bond polarity of all bond types and the formal restrictions of the multipole model, which are visible in the residual density analysis the considerably high overall-agreement between the theoretically obtained multipole model *cry* and the multipole-free models *pck*-s and *pck*-l supports the assumption of a sufficient reliability of the derived physical properties and the underlying ED of all models.

Theoretical Calculations and Refinement Procedures

The experimental crystal structure[28] was used as starting model for a geometry optimization with periodic boundary conditions using the program Crystal06[61], see Figure 1A. The basis sets were chosen from the Crystal06 Basis Sets Library to balance each other. They were at least of polarized double zeta quality: hydrogen: 3-1p1G[62], nitrogen: 6-21G*[63], boron: 6-21G*.[64] With the program Properties06 of the Crystal06 program package, theoretical structure factors corresponding to the experimental resolution were calculated. In a subsequent XD refinement[65] a theoretical ED model (cry) including intermolecular interactions was obtained. The imposed symmetries are 43*m* for nitrogen atoms and 4*mm* for boron atoms. The general refinement procedure was: (i) Initial charge separation such that the sums of the monopoles refer to the ideal charges of –2 for the B_6H_6 part and +1 for the NH_4 part. In this study, only the monopoles of the protic and hydridic hydrogen atoms were adjusted to obtain the charge separation. Refinement of scale factor: (ii) Refinement of multipoles with fixed charge separation for anion and cation. (iii) Release of charge restriction between borate and ammonium. (iv) Inclusion of κ for N and B. (v) Blockwise refinement of κ and κ_0 for all atoms.

Additionally, gas phase calculations were performed. Since $(B_6H_6)^{2-}$ is not stable in the gas phase, two clusters were generated; one includes the eight ammonium ions of the first coordination sphere, the larger one contains 13 borate cages and 32 ammonium ions. For these models (*pck*-s and *pck*-l), single point calculations were performed at the B3LYP/6-311+g(2d,2p) level of theory using Gaussian03.[66] The wavefunctions were analyzed with AIM2000[67] and DGRID-4.5.[68] For the grid calculations, a step size of 0.05 bohr was applied. These multipole-free models serve as references for model *cry*. Since the wavefunction-file of model *pck*-l is very large, some of the integrated bond descriptors, such as the delocalization index and the ELI-D, were calculated only for model *pck*-s. For instance, the integration of an atomic basin with AIM2000 is not feasible for model *pck*-l.

The experimental structure of data set 1 was displayed with Mercury[69], the first coordination sphere of $(B_6H_6)^{2-}$ with GaussView[66], the large packing scheme with Schakal.[70] Deformation densities, Laplacians, Hirshfeld Surfaces, and the ELI-D were displayed with MolIso.[71] The AIM-topology was displayed with AIM2000.[67]

Supporting Information (see footnote on the first page of this article): Supporting information contains the packing scheme within the unit cell, the progression of rho along the crystallographic 100, 110, and 111 directions (model *cry*), the expansion parameters for model *cry*, and the quantitative ELI-D results of model *pck*-s.

Acknowledgements

We thank the Deutsche Forschungsgemeinschaft (DFG grants LE423/13–3 and LU222/30–2 within SPP1178 and grant HE 4573/3–1) for financial support. *Beate Paulus* is acknowledged for helpful discussions.

References

[1] G. N. Lewis, *Valence and the Structure of Atoms and Molecules*, The Chemical Catalogue Co., New York, **1923**.
[2] W. N. Lipscomp, *Boron Hydrides*, Benjamin, New York, **1963**.
[3] K. Wade, *J. Chem. Soc. Chem. Commun.* **1971**, 792–793.
[4] D. A. Dixon, D. A. Kleier, T. A. Halgren, J. H. Hall, W. N. Lipscomp, *J. Am. Chem. Soc.* **1977**, *99*, 6226–6237.
[5] R. B. King, D. H. Rouvray, *J. Am. Chem. Soc.* **1977**, *99*, 7834–7840.
[6] A. Stone, *Mol. Phys.* **1980**, *41*, 1339–1354.
[7] E. D. Jemmis, *J. Am. Chem. Soc.* **1982**, *104*, 7017–7020.
[8] a) R. E. Williams, *Chem. Rev.* **1992**, *92*, 177–207; b) A. J. C. Wilson, *International Tables of Crystallography*, Vol. C, Kluver Academic Publishers, Boston, **1992**.
[9] R. B. King, *Chem. Rev.* **2001**, *101*, 1119–1152.
[10] P. Hohenberg, W. Kohn, *Phys. Rev.* **1964**, *136*, 864–871.
[11] R. F. Stewart, *J. Phys. Chem.* **1969**, *73,* 4569–4577.
[12] N. K. Hansen, P. Coppens, *Acta Crystallogr. Sect. A* **1978**, *34*, 909–921.
[13] R. Brill, H. Dietrich, H. Dierks, *Acta Crystallogr., Sect. B* **1971**, *27*, 2003–2018.
[14] H. Dietrich, C. Scheringer, *Acta Crystallogr., Sect. B* **1978**, *34*, 54–63.
[15] C. T. Chantler, E. N. Maslen, *Acta Crystallogr., Sect. B* **1989**, *45*, 290–297.
[16] M. Yu. Antipin, A. V. Poliakov, M. Kapphan, V. G. Tsirelson, R. P. Ozerov, Y. T. Struchkov, *Organomet. Chem. USSR* **1990**, *3*, 421–426.
[17] M. Antipin, R. Boese, D. Bläser, A. Maulitz, *J. Am. Chem. Soc.* **1997**, *119*, 326–333.
[18] K. A. Lyssenko, M. Yu. Antipin, V. N. Lebedev, *Inorg. Chem.* **1998**, *37*, 5834–5843.
[19] I. V. Glukhov, K. A. Lyssenko, A. A. Korlyukov, M. Yu. Antipin, *Russ. Chem. Bull. Int. Ed.* **2005**, *54*, 547–559.
[20] K. A. Lyssenko, D. G. Golovanov, V. I. Meshcheryakov, A. R. Kudinov, M. Yu. Antipin, *Russ. Chem. Bull. Int. Ed.* **2005**, *54*, 933–941.
[21] I. V. Glukhov, K. A. Lyssenko, M. Yu. Antipin, *Struct. Chem.* **2007**, *18*, 465–469.
[22] I. V. Glukhov, K. A. Lyssenko, A. A. Korlyukov, M. Yu. Antipin, *Faraday Discuss.* **2007**, *135*, 203–215.
[23] D. Förster, S. Scheins, P. Luger, D. Lentz, W. Preetz, *Eur. J. Inorg. Chem.* **2007**, *20*, 3169–3172.

Special Issue

[24] a) D. Förster, C. B. Hübschle, P. Luger, T. Hügle, D. Lentz, *Inorg. Chem.* **2008**, *47*, 1874–1876; b) . M. Panda, K. Hofmann, M. H. Prosenc, B. Albert, *Dalton Trans.* **2008**, 3956–3958.
[25] S. Mebs, R. Kalinowski, S. Grabowsky, D. Förster, R. Kickbusch, E. Justus, W. Morgenroth, C. Paulmann, P. Luger, D. Gabel, D. Lentz, *Inorg. Chem.* **2010**, *49*, 90–103.
[26] S. Mebs, R. Kalinowski, S. Grabowsky, D. Förster, R. Kickbusch, E. Justus, W. Morgenroth, C. Paulmann, P. Luger, D. Gabel, D. Lentz, *J. Phys. Chem. A* **2011**, *115*, 1385–1395.
[27] R. F. W. Bader, D. A. Legare, *Can. J. Chem.* **1992**, *70*, 657–676.
[28] Crystal data for: $H_{14}B_6N_2$, M = 106.99, cubic, a = 9.0970(10) Å, V = 752.83(14) Å^3, T = 98(2) K, space group $Fm\bar{3}m$, Z = 4, Mo-K_a, 18867 reflections measured, 415 independent reflections (R_{int} = 0.0175). The final R_1 = 0.0237 [$I > 2\sigma(I)$], $wR(F^2)$ = 0.0685 (all data). GOOF = 1.235. Further details of the crystal structure investigation may be obtained from the Fachinformationszentrum Karlsruhe, 76344 Eggenstein-Leopoldshafen, Germany (Fax: +49-7247-808-666; E-Mail: crysdata@fizkarlsruhe. *de*, http://www.fiz-karlsruhe.de/request for deposited data.html) on quoting the depository number CSD-426324.
[29] R. F. W. Bader, *Atoms in Molecules. A Quantum Theory*, Cambridge University Press, Oxford U. K., **1991**.
[30] R. F. W. Bader in *The Enzyclopedia of Computational Chemistry*, (Eds.: P. von R. Schleyer, N. L. Alinger, T. Clark, J. Gasteiger, P. A. Kollman, H. F. Schaefer III, P. R. Schreiner), Wiley, Chichester, **1998**.
[31] F. L. Hirshfeld, *Theor. Chim. Acta* **1977**, *44*, 129–139.
[32] M. A. Spackman, P. G. Byrom, *Chem. Phys. Lett.* **1997**, *267*, 215–220.
[33] R. F. W. Bader, M. E. Stephens, *J. Am. Chem. Soc.* **1975**, *97*, 7391–7399.
[34] X. Fradera, M. A. Austen, R. F. W. Bader, *J. Phys. Chem. A* **1999**, *103*, 304–314.
[35] R. F. W. Bader, C. Gatti, *Chem. Phys. Lett.* **1998**, *287*, 233–238.
[36] C. Gatti, F. Cargnoni, L. Bertini, *J. Comput. Chem.* **2003**, *24*, 422–436.
[37] C. Gatti, L. Bertini, *Acta Crystallogr., Sect. A* **2004**, *60*, 438–449.
[38] M. Kohout, *Int. J. Quantum Chem.* **2004**, *97*, 651–658.
[39] A. D. Becke, K. E. Edgecombe, *J. Chem. Phys.* **1990**, *92*, 5397–5403.
[40] B. Silvi, A. Savin, *Nature* **1994**, *371*, 683–686.
[41] M. Kohout, A. Savin, *Int. J. Quantum Chem.* **1996**, *60*, 875–882.
[42] A. Burkhardt, U. Wedig, H. G. von Schnering, A. Savin, *Z. Anorg. Allg. Chem.* **1993**, *619*, 437–441.
[43] T. F. Fässler, A. Savin, *Chem. unserer Zeit* **1997**, *31*, 110–120.
[44] A. Savin, R. Nesper, S. Wengert, T. F. Fässler, *Angew. Chem.* **1997**, *109*, 1892–1918.
[45] H. Binder, R. Kellner, K. Vaas, M. Hein, F. Baumann, M. Wanner, W. Kaim, U. Wedig, W. Hönle, H. G. von Schnering, O. Groeger, G. Engelhardt, *Z. Anorg. Allg. Chem.* **1999**, *625*, 1638–1646.
[46] M. Yamaguchi, Y. Ohishi, S. Hosoi, K. Soga, K. Kimura, *J. Phys. Conf. Ser.* **2009**, *148*, 012027.
[47] N. Peres, A. Boukhris, M. Souhassou, G. Gaboille, C. Lecomte, *Acta Crystallogr., Sect. A* **1999**, *55*, 1038–1048.
[48] J. J. Bentley, R. F. Stewart, *Acta Crystallogr., Sect. A* **1976**, *32*, 910–914.
[49] A. Volkov, Y. Abramov, P. Coppens, C. Gatti, *Acta Crystallogr., Sect. A* **2000**, *56*, 332–339.
[50] A. Volkov, Y. Abramov, P. Coppens, *Acta Crystallogr., Sect. A* **2001**, *57*, 272–282.
[51] K. Meindl, J. Henn, *Residual Density Analysis*, in *Series Structure and Bonding: Electron Density and Chemical Bonding II - Theoretical Charge Density Studies*; Springer Berlin-Heidelberg, **2012**, p. 143–192.
[52] S. C. Abrahams, E. T. Keve, *Acta Crystallogr., Sect. A* **1971**, *27*, 157–165.
[53] K. Meindl, J. Henn, *Acta Crystllogr. Sect. A* **2008**, *64*, 404–418.
[54] A. O. Borissova, M. Yu. Antipin, K. A. Lyssenko, *J. Phys. Chem. A* **2009**, *113*, 10845–10851.
[55] L. J. Farrugia, C. Evans, D. Lentz, M. Roemer, *J. Am. Chem. Soc.* **2009**, *131*, 1251–1268.
[56] S. Mebs, M. Chilleck, S. Grabowsky, T. Braun, *Chem. Eur. J.* **2012**, *18*, 11647–11661.
[57] The theoretical calculations were performed in reduced *C*2*v* symmetry due to software limitations. Hence it is not surprising that the theoretical calculations break the cubic symmetry. A tiny numerical random difference, e.g. from roundoff errors, in model parameters or atomic coordinates may cause this.
[58] S. J. Grabowski, *Relationships between QTAIM and the Decomposition of the Interaction Energy - Comparison of Different Kinds of Hydrogen Bond. The Quantum Theory of Atoms in Molecules*, Wiley-VCH, Weinheim, **2007**, ch. 17.2, pp. 456–459.
[59] R. F. W. Bader, *J. Phys. Chem. A* **1998**, *102*, 7314–7323.
[60] S. Mebs, S. Grabowsky, D. Forster, R. Kickbusch, M. Hartl, L. L. Daemen, W. Morgenroth, P. Luger, B. Paulus, D. Lentz, *J. Phys. Chem. A* **2010**, *114*, 10185–10196.
[61] R. Dovesi, V. R. Saunders, C. Roetti, R. Orlando, C. M. Zicovich-Wilson, F. Pascale, B. Civalleri, K. Doll, N. Harrison, I. J. Bush, Ph. D'Arko, M. Llunell, *CRYSTAL06, version 1.0.2.*, User's Manual, **2006**, University of Torino.
[62] C. Gatti, V. R. Saunders, C. Roetti, *J. Chem. Phys.* **1994**, *101*, 10686–10696.
[63] R. Dovesi, M. Causa', R. Orlando, C. Roetti, V. R. Saunders, *J. Chem. Phys.* **1990**, *92*, 7402–7411.
[64] R. Orlando, R. Dovesi, C. Roetti, V. R. Saunders, *J. Phys. Condens. Matter* **1990**, *2*, 7769–7789.
[65] A. Volkov, P. Macchi, L. J. Farrugia, C. Gatti, P. Mallinson, T. Richter, T. Koritsanszky, *XD2006*: A Computer Program for Multipole Refinement, Topological Analysis of Charge Densities and Evaluation of Intermolecular Energies from Experimental or Theoretical Structure Factors, User Manual, **2006**.
[66] Gaussian 03, Revision C.02, M. J. Frisch, G. W. Trucks, H. B. Schlegel, G. E. Scuseria, M. A. Robb, J. R. Cheeseman, J. A. Montgomery Jr., T. Vreven, K. N. Kudin, J. C. Burant, J. M. Millam, S. S. Iyengar, J. Tomasi, V. Barone, B. Mennucci, M. Cossi, G. Scalmani, N. Rega, G. A. Petersson, H. Nakatsuji, M. Hada, M. Ehara, K. Toyota, R. Fukuda, J. Hasegawa, M. Ishida, T. Nakajima, Y. Honda, O. Kitao, H. Nakai, M. Klene, X. Li, J. E. Knox, H. P. Hratchian, J. B. Cross, V. Bakken, C. Adamo, J. Jaramillo, R. Gomperts, R. E. Stratmann, O. Yazyev, A. J. Austin, R. Cammi, C. Pomelli, J. W. Ochterski, P. Y. Ayala, K. Morokuma, G. A. Voth, P. Salvador, J. J. Dannenberg, V. G. Zakrzewski, S. Dapprich, A. D. Daniels, M. C. Strain, O. Farkas, D. K. Malick, A. D. Rabuck, K. Raghavachari, J. B. Foresman, J. V. Ortiz, Q. Cui, A. G. Baboul, S. Clifford, J. Cioslowski, B. B. Stefanov, G. Liu, A. Liashenko, P. Piskorz, I. Komaromi, R. L. Martin, D. J. Fox, T. Keith, M. A. Al-Laham, C. Y. Peng, A. Nanayakkara, M. Challacombe, P. M. W. Gill, B. Johnson, W. Chen, M. W. Wong, C. Gonzalez, J. A. Pople, Gaussian, Inc., Wallingford CT, 2004.
[67] *AIM2000* – A Program to Analyze and Visualize Atoms in Molecules: F. Biegler-Konig, J. Schönbohm, D. Bayles, *J. Comput. Chem.* **2001**, *22*, 545–559.
[68] M. Kohout, DGRID, version 4.5, Radebeul, 2009.
[69] C. F. Macrae, P. R. Edgington, P. McCabe, E. Pidcock, G. P. Shields, R. Taylor, M. Towler, J. van de Streek, *J. Appl. Crystallogr.* **2006**, *39*, 453–457; IUCr macros version 2.1.2: 2010/05/13; http://www.ccdc.cam.ac.uk/mercury.
[70] E. Keller, J.-S. Pierrard, *SCHAKAL99*, A Fortran Program for the Graphical Representation of Molecular and Solid-State Structure Models, Albert Ludwigs Universitat Freiburg, Germany.
[71] MolIso – A Program for Colour-Mapped Iso-Surfaces: C. B. Hübschle, P. Luger, *J. Appl. Crystallogr.* **2006**, *39*, 901–904.

Received: November 9, 2012
Published Online: June 27, 2013

